

# Azimuthally-sensitive femtoscopy from RHIC to LHC in hydrodynamics with statistical hadronization\*

Adam Kisiel,<sup>1,2,†</sup> Wojciech Broniowski,<sup>3,4,‡</sup> Mikolaj Chojnacki,<sup>3,§</sup> and Wojciech Florkowski<sup>3,4,¶</sup>

<sup>1</sup>*Faculty of Physics, Warsaw University of Technology, PL-00661 Warsaw, Poland*

<sup>2</sup>*Department of Physics, Ohio State University, 1040 Physics Research Building,  
191 West Woodruff Ave., Columbus, OH 43210, USA*

<sup>3</sup>*The H. Niewodniczański Institute of Nuclear Physics,  
Polish Academy of Sciences, PL-31342 Kraków, Poland*

<sup>4</sup>*Institute of Physics, Jan Kochanowski University, PL-25406 Kielce, Poland*

(Dated: 24 August 2008)

Azimuthally-sensitive femtoscopy for heavy-ion collisions at RHIC and LHC is explored within the approach consisting of the hydrodynamics of perfect fluid followed by statistical hadronization. It is found that for the RHIC initial conditions the very same framework that reproduces the standard soft observables (including the transverse-momentum spectra, the elliptic flow, and the azimuthally-averaged HBT radii) leads to a proper description of the azimuthally-sensitive femtoscopic observables - we find that the azimuthal variation of the *side* and *out* HBT radii is very well reproduced for all centralities, while the *out-side* correlation is somewhat too large for non-central events. Concerning the dependence of the femtoscopic parameters on  $k_T$  we find that it is very well reproduced for the *out* and *side* radii, and fairly well for the *long* radius. The model is then extrapolated for the LHC energy. We predict the overall moderate growth of the HBT radii and the decrease of their azimuthal oscillations. Such effects are naturally caused by longer evolution times. In addition, we discuss in detail the space-time patterns of particle emission. We show that they are quite complex and argue that the overall shape seen by the femtoscopic methods cannot be easily disentangled on the basis of simple-minded arguments.

PACS numbers: 25.75.-q, 25.75.Dw, 25.75.Ld

Keywords: relativistic heavy-ion collisions, hydrodynamics, femtoscopy, HBT correlations, azHBT, RHIC, LHC

## I. INTRODUCTION

Femtoscopy provides detailed information on the dynamics of systems formed in relativistic heavy-ion collisions (for a review and literature see [1]). In particular, the Hanbury-Brown-Twiss (HBT) [2, 3, 4, 5] intensity interferometry exhibits sensitivity to shape and flow of the medium at freeze-out, which in turn reflects the conditions throughout the evolution, from the formation till the cease of interactions. Together with other observed quantities, such as the ratios of particle abundances, momentum spectra, the elliptic flow coefficient, or other correlation data, femtoscopy contributes to the growing precise knowledge of the dynamics of the system. Azimuthally sensitive HBT interferometry (azHBT) [6, 7], which is the subject of this paper, brings in information on the dependence of shape and flow on the azimuthal angle  $\phi$ . This information is complementary to the data on the transverse-momentum elliptic coefficient  $v_2$  [8], which is a measure of the azimuthal asymmetry of the

flow. Thus, a simultaneous description of azHBT and  $v_2$  verifies consistency of the theoretical description.

In this work we use what we call the *standard approach*, consisting of ideal-fluid hydrodynamics followed by statistical hadronization. Numerous calculations have been done in this framework, with the common difficulty [9] of simultaneously describing femtoscopy and other signatures of the data. More precisely, the *RHIC HBT puzzle* [1, 9, 10, 11] refers to problems in reconciling the large value of the elliptic flow coefficient,  $v_2$ , with the HBT interferometry in calculations based on hydrodynamics [12, 13, 14, 15, 16]. In the standard approach the description of  $v_2$  requires longer hydrodynamic evolution times, while the HBT radii, sensitive to the size and lifetime of the system, are properly reproduced when the lifetime of the system is short. The two requirements are in conflict. Due to the obstacle of the RHIC HBT puzzle, only few calculations or physically motivated parametrization of the azHBT quantities have been made [17, 18, 19, 20, 21, 22, 23]. Moreover, in our view the comparison to data of the azimuthal dependence of the correlation radii makes sense only when the values averaged over  $\phi$  are also properly reproduced.

Recently, we have accomplished a successful uniform description of soft observables at RHIC, including the HBT radii, within the standard approach [24]. The essential ingredients of this analysis are the Gaussian initial condition for hydrodynamics, early start of the evolution, the state-of-the art equation of state with smooth

---

\*Supported in part by the Polish Ministry of Science and Higher Education, grants N202 153 32/4247, N202 034 32/0918, N202 249235, and by the U.S. NSF grant no. PHY-0653432.

<sup>†</sup>Electronic address: kisiel@if.pw.edu.pl

<sup>‡</sup>Electronic address: Wojciech.Broniowski@ifj.edu.pl

<sup>§</sup>Electronic address: Mikolaj.Chojnacki@ifj.edu.pl

<sup>¶</sup>Electronic address: Wojciech.Florkowski@ifj.edu.pl

crossover, and the use of THERMINATOR [25] with all resonances from SHARE [26] incorporated to carry out the statistical hadronization at the freeze-out surface of temperature 145 MeV. The interplay of these elements resulted in a simultaneous description of the transverse-momentum spectra of pions, kaons and protons, the  $v_2$ , and the HBT correlation radii of pions, including the basic azHBT signatures. The agreement of this quality cannot be achieved with the initial condition obtained from the typically used Glauber models. In that case the HBT radii, in particular the ratio of *out* to *side* radii, is reproduced at the level of 20% only [27]. The reader is referred to Ref. [24] for the details.

In this paper we present a systematic study of the azimuthally sensitive HBT radii in the model of Ref. [24], including the dependence on centrality and the transverse momentum of the pair,  $k_T$ . We find that the azimuthal variation of the *side* and *out* radii is properly reproduced for all centralities, while in the case of the *out-side* correlation it is somewhat too large for non-central events. Concerning the dependence of the femtosopic parameters on  $k_T$ , it is very well reproduced for the *out* and *side* radii, and fairly well for the *long* radius. We stress that the present study involves no parametric freedom, as all parameters have been fixed in the global fits of Ref. [24].

Next, we extrapolate the model to the LHC energy, where predictions for the HBT and azHBT quantities is made. In addition, we present a detailed analysis of the space-time patterns of the pion emission. We argue that this emission, consisting of surface and volume parts, exhibits a rather complex behavior. We argue that the determination of the overall shape of the source seen by the femtosopic methods is not straightforward and requires detailed simulation, such as the one performed in this work.

We use  $c = 1$  throughout the paper. The label RHIC denotes the AuAu collisions at the highest RHIC energy of  $\sqrt{s_{NN}} = 200$  GeV, while LHC corresponds to the PbPb collisions at  $\sqrt{s_{NN}} = 5500$  GeV.

## II. THE FRAMEWORK

In this section we describe the essential elements of our method to the extent they are necessary for the comprehensive presentation of the new results. More details concerning the hydrodynamics can be found in Refs. [24, 28, 29], while the method used for femtosopic calculations has been presented in great detail in Ref. [30].

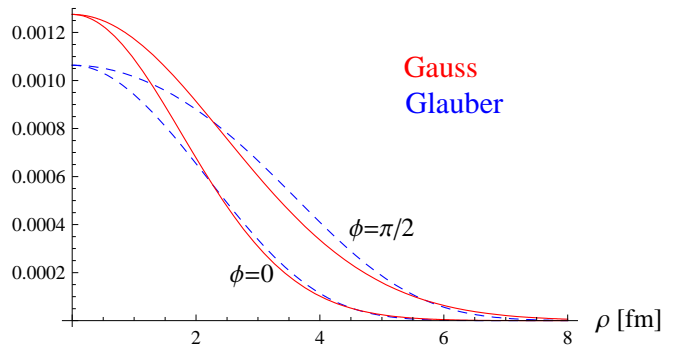


FIG. 1: (Color online) In-plane and out-of-plane sections of the two-dimensional energy-density profiles for  $c = 30 - 40\%$  obtained from the mixed Glauber model described in the text (dashed lines) and the Gaussian parametrization (1) used in this work (solid lines). Both profiles are normalized to unity, and in addition  $\langle x^2 \rangle = a^2$ ,  $\langle y^2 \rangle = b^2$ .

### A. Initial condition

As reported in Ref. [24], the use of the initial condition for hydrodynamics of the Gaussian form,

$$n(x, y) = \exp\left(-\frac{x^2}{2a^2} - \frac{y^2}{2b^2}\right), \quad (1)$$

where  $x$  and  $y$  denote the transverse coordinates, leads to a much better uniform description of the data for the  $p_T$ -spectra,  $v_2$ , and the pionic HBT radii compared to the use of the standard initial condition from the Glauber model.

The width parameters  $a$  and  $b$  depend on centrality. In order to use realistic values we run the GLISSANDO [31] Glauber Monte Carlo simulations which include the eccentricity fluctuations [32, 33]. Then we match  $a^2$  and  $b^2$  to reproduce the values  $\langle x^2 \rangle$  and  $\langle y^2 \rangle$  from the GLISSANDO profiles. Thus, by construction, the spatial rms radii of the initial condition and its eccentricity is the same as from the Glauber calculation. Nevertheless, the shape is not the same, as is evident from Fig. 1. The Gaussian profiles are sharper near the origin, which results in a faster buildup of the Hubble-like flow in the hydrodynamical stage. Admittedly, the initial density and flow profiles should eventually be obtained from the early dynamics, such as the Color Glass Condensate theory [34, 35, 36]. In practice, however, modeling of the partonic stage carries uncertainty in its parameters. In addition, other effects in the early dynamics are present, see e.g. [37, 38], making precise profile calculations difficult. Thus the use of a simple parametrization of the initial profile is a profitable and practical approach, while the need remains for its detailed dynamical justification.

The Glauber calculations, needed to obtain the  $a$  and  $b$  parameters, correspond to the mixed model [39], where the number of produced particles is proportional to  $(1 - \alpha)N_w/2 + \alpha N_{\text{bin}}$ , with  $N_w$  and  $N_{\text{bin}}$  denoting the number of wounded nucleons [40] and binary collisions,

TABLE I: Shape parameters  $a$  and  $b$  of Eq. (1) for various centrality classes obtained by matching  $\langle x^2 \rangle$  and  $\langle y^2 \rangle$  to GLISSANDO simulations, the variable-axes eccentricity  $\epsilon^*$ , and the chosen central temperature  $T_i$ .

$c$ [%]	0-5	5-10	10-20	20-30	30-40	40-50	50-60	60-70	70-80
	RHIC								
$a$ [fm]	2.70	2.54	2.38	2.00	1.77	1.58	1.40	1.22	1.04
$b$ [fm]	2.93	2.85	2.74	2.59	2.45	2.31	2.16	2.02	1.85
$\epsilon^*$	0.08	0.12	0.18	0.25	0.31	0.36	0.41	0.46	0.52
$T_i$ [MeV]	330	325	315	305	285	260	230	205	185
	LHC								
$a$ [fm]	2.65	2.47	2.22	1.95	1.73	1.56	1.40	1.24	1.06
$b$ [fm]	2.89	2.80	2.69	2.55	2.41	2.28	2.15	2.02	1.85
$\epsilon^*$	0.09	0.12	0.19	0.26	0.32	0.36	0.40	0.45	0.51
$T_i$ [MeV]	500	500	500	500	500	500	500	500	500

respectively. The parameter  $\alpha = 0.145$  for RHIC [41, 42] and is set by us to 0.2 for LHC. The inelastic nucleon cross section is 42 mb for RHIC and 63 mb for LHC [43]. The simulations incorporate the fluctuations of orientation of the fireball (the variable-axes geometry), which result in increased eccentricity compared to the fixed-axes geometry [44]. Finally, the expulsion distance of 0.4 fm is used in the generation of the nuclear distributions, and the source-dispersion parameter of 0.7 fm is used. This parameter describes the random displacement of the source from the center of the wounded nucleon or the binary-collision position [31]. The values of the  $a$  and  $b$  parameters for various centralities and the corresponding eccentricity parameters

$$\epsilon^* = \frac{b^2 - a^2}{a^2 + b^2}, \quad (2)$$

are collected in Table I.

The energy-density profile (1) determines the initial temperature profile via the equation of state [29]. The initial central temperature,  $T_i$ , is a model parameter dependent on centrality. For RHIC calculations it is adjusted to reproduce the total particle multiplicity. For the LHC we use for simplicity a common value of 500 MeV. When the LHC multiplicity data are available in the future, this parameter will be tuned more realistically.

## B. Hydrodynamics

The hydrodynamic equations used in this work were described in detail in Refs. [28, 29]. We use inviscid (ideal-fluid), baryon-free, boost-invariant hydrodynamics. The equations are written in terms of the velocity of sound,  $c_s$ , whose temperature dependence encodes the full information on the equation of state of the system. Importantly, we incorporate the known features of  $c_s(T)$ , which at high temperatures are given by the lattice QCD calculations, at low  $T$  follow from the hadron

gas including all resonances, while in between an interpolation is used. Importantly, no phase transition, but a smooth cross-over is built in, in accordance to the present knowledge of the thermodynamics of QCD at zero baryon chemical potential. The plot of the resulting  $c_s(T)$  can be found in Ref. [24].

The initial proper time for the start of hydrodynamics is fixed to have the value

$$\tau_0 = 0.25 \text{ fm} \quad (3)$$

for all centralities, both for RHIC and LHC. This early start of hydrodynamics allows for a fast generation of transverse flow.<sup>1</sup>

## C. Freeze-out

The hydrodynamic evolution proceeds until the freeze-out occurs, where the assumed condition for the *universal* freeze-out temperature is  $T_f = 145$  MeV. This value is somewhat lower than in several fits of the chemical freeze-out [45, 46, 47], however, it agrees with the recently made global fits to particle transverse momentum spectra of Ref. [48, 49], where the value around 145 MeV was obtained for the kinetic freeze-out temperature.<sup>2</sup>

The freeze-out hypersurfaces are compared in Fig. 2. We use the centrality 20-30% as an example, as for other cases the results are qualitatively similar. The left and middle panels show the role of the initial condition used

<sup>1</sup> The ignition of hydrodynamics may be delayed to later times, about 1 fm, if it is preceded with particle free-streaming starting at 0.25 fm followed by the Landau matching [24]. This mechanism generates some initial flow (transverse and elliptic) for hydrodynamics. The resulting freeze-out hypersurfaces are very close to those used in this work.

<sup>2</sup> The use of this lower freeze-out temperature needs the introduction of the strangeness inequilibrium factors  $\gamma_s$  in order to reproduce the abundances of strange particles [48].

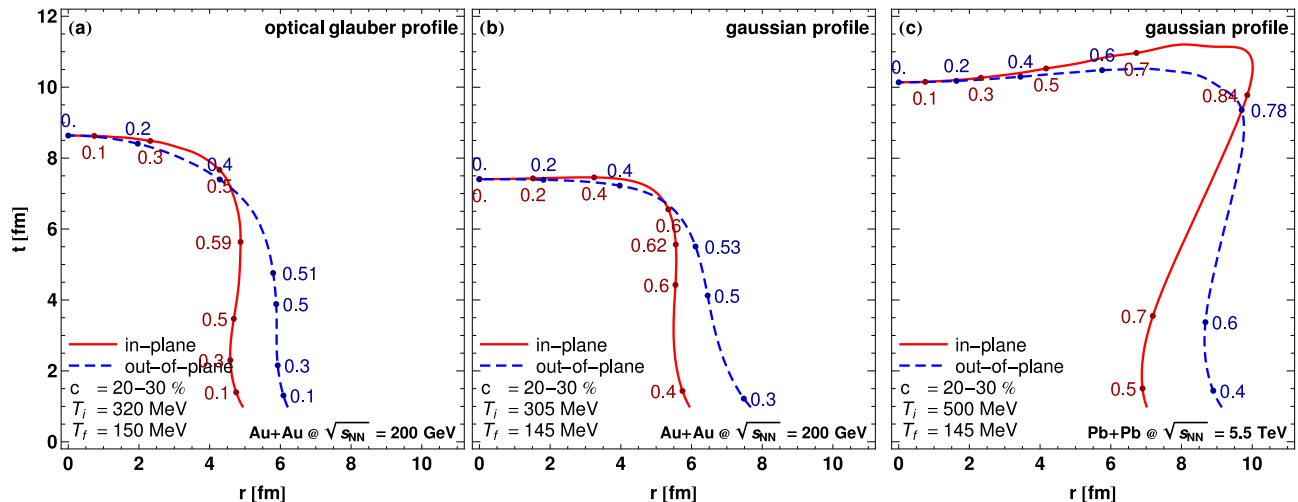


FIG. 2: (Color online) Sections of the freeze-out hypersurfaces for the Glauber initial condition used in Ref. [27] (left) and for the Gaussian initial condition (middle) for centrality 20-30% for RHIC, and for the Gaussian initial condition for centrality 20-30% for LHC (right). The dots with numbers indicate the values of the transverse velocity at freeze-out.

for the RHIC analysis. For the Glauber initial condition used in Ref. [27] (left) the freeze-out hypersurface is smaller in transverse size but longer in the life-time than for the case of the Gaussian initial condition (middle) used in the present work. Parameters in both calculations were optimized to reproduce the yields, the  $p_T$  spectra, and  $v_2$ . The fact that for the Gaussian initial profile the source has a significantly larger transverse size and shorter emission time is a crucial feature for the successful description of the HBT data.

The freeze-out hypersurfaces have the *volume* emission parts (with time-like normal vectors, i.e. running approximately flat in Fig. 2), which are similar to the blast-wave parametrization [50]. The lifetime is short: about 9 fm for central ( $c = 0-5\%$ ) and 7 fm for mid-peripheral ( $c = 20-30\%$ ) collisions at RHIC. However, they also contain the *surface* emission parts (with space-like normal vectors, i.e. running more-or-less vertical in Fig. 2), absent in the usual blast-wave parametrizations. Nevertheless, there is no problem with the non-causal surface emission [51, 52, 53], which is negligible, since less than 0.5% of particles are emitted back into the hydrodynamic region. This very small fraction follows from the large transverse flow velocity at large radii, as indicated by the labels in Fig. 2. This large flow carries the particles outward. In addition, for the RHIC case the hypersurfaces are not bent back at low times, as occurs in some hydrodynamic calculations. Quantitatively, we have found that about half of the produced particles comes from the volume emission part and about half from the surface emission part. The relevance of the surface emission is also stressed in Refs. [54, 55].

The right panel in Fig. 2 shows the freeze-out hypersurface for the LHC extrapolation for the Gaussian initial profile and the same centrality. We note a larger transverse size and emission times compared to the RHIC case of the middle panel. The surface-emission parts of the

curves are bent back, but at the same time the expansion velocity is larger, such that the backward emission problem is again irrelevant.

THERMINATOR is used to carry out the statistical hadronization at the freeze-out hypersurface according to the Cooper-Frye formulation [56]. According to the assumed single-freeze-out approximation, identifying the kinetic and chemical freeze-out temperatures, rescattering process after freeze-out are neglected. We have checked that the collision rate after freeze-out is moderate for the hypersurfaces applied in this work. We estimate it by considering a pion straight-line trajectory and counting the number of encounters with other particles closer than the distance corresponding to the pion-hadron cross section. The average number of these trajectory crossings is about 1.5-1.7 per pion. This shows that the single-freeze-out approximation [46] works reasonably well for the present case. At a more detailed level, one could use hadronic afterburners to model the elastic collisions [57, 58, 59], or attempt the hydro-kinetic approach implemented in [60].

#### D. Model parameters

For the reader's convenience, we list here again all the model parameters. The model has the total of 5 parameters. Parameters dependent on the centrality classes are the Gaussian widths,  $a$ ,  $b$ , and the initial central temperature,  $T_i$ . The widths are fixed with GLISSANDO [31], while  $T_i$  is adjusted in order to reproduce the particle multiplicities. The parameters independent of centrality are the starting proper time of hydrodynamics,  $\tau_0$ , and the universal freeze-out temperature,  $T_f$ .

## E. Two-particle femtoscopy

The method of dealing with the HBT quantities has been thoroughly described in Ref. [30], where the reader is referred to for details. Here we only note that our technique follows exactly the experimental procedure of extracting the femtoscopic quantities, including the passage to the LCMS (local co-moving system) frame, the application of the two-particle method, and carrying out the Bowler-Sinyukov procedure [61, 62] to incorporate the Coulomb corrections.

We use the standard Pratt-Bertsch parametrization [63, 64]. For the case without azimuthal symmetry the correlation function is fitted to the formula including the cross terms between the HBT radii [65]:

$$C(q_{\text{out}}, q_{\text{side}}, q_{\text{long}}) = 1 + \lambda \exp(-R_{\text{out}}^2 q_{\text{out}}^2 - R_{\text{side}}^2 q_{\text{side}}^2 - R_{\text{long}}^2 q_{\text{long}}^2 - R_{\text{out-side}} q_{\text{out}} q_{\text{side}} - R_{\text{out-long}} q_{\text{out}} q_{\text{long}} - R_{\text{side-long}} q_{\text{side}} q_{\text{long}}) \quad (4)$$

The basic quantities of the azimuthally sensitive HBT analysis are the second-order Fourier coefficients defined as

$$\begin{aligned} R_{\text{out}}^2(\phi) &= R_{\text{out},0}^2 + 2R_{\text{out},2}^2 \cos(2\phi), \\ R_{\text{side}}^2(\phi) &= R_{\text{side},0}^2 + 2R_{\text{side},2}^2 \cos(2\phi), \\ R_{\text{long}}^2(\phi) &= R_{\text{long},0}^2 + 2R_{\text{long},2}^2 \cos(2\phi), \\ R_{\text{out-side}}(\phi) &= 2R_{\text{out-side},2} \sin(2\phi), \\ R_{\text{out-long}}(\phi) &= 2R_{\text{out-long},2} \cos(2\phi), \\ R_{\text{side-long}}(\phi) &= 2R_{\text{side-long},2} \sin(2\phi). \end{aligned} \quad (5)$$

## III. RESULTS

### A. RHIC

In Fig. 3 we present the summary of our results compared to the experimental data from the STAR AuAu collisions at  $\sqrt{s_{NN}} = 200$  AGeV [66]. The figure shows the centrality and pair transverse momentum ( $k_T$ ) dependence. For each centrality, associated here with the number of participants  $N_{\text{part}}$  on the horizontal axis, we plot the experimental points (filled dots) and the model results (empty symbols). The points from top to bottom correspond to  $k_T$  contained in the bins of 0.15-0.25 GeV, 0.25-0.35 GeV, and 0.35-0.6 GeV. The top panels show the radii squared averaged over the  $\phi$  angle, from left to right,  $R_{\text{out},0}^2$ ,  $R_{\text{side},0}^2$ , and  $R_{\text{long},0}^2$ . The bottom panels show the magnitude of the allowed oscillations divided by  $R_{\text{side},0}^2$ , which is the adopted convention used in presenting the experimental data.

The values of the model points in the plots were obtained by first solving the hydrodynamic equations and running THERMINATOR as described in the previous sections. Then, according to our procedure, 144 separate correlation functions have been constructed (6 centrality bins  $\times$  4  $k_T$  bins  $\times$  6 bins for the phi angle). The

$\phi$  dependence of the correlation function was obtained in the following way: an angle between the  $k_T$  direction and the reaction plane was determined and the pairs were grouped into six bins:  $(-\frac{\pi}{12}, \frac{\pi}{12})$ ,  $(\frac{\pi}{12}, \frac{3\pi}{12})$ ,  $(\frac{3\pi}{12}, \frac{5\pi}{12})$ ,  $(\frac{5\pi}{12}, \frac{7\pi}{12})$ ,  $(\frac{7\pi}{12}, \frac{9\pi}{12})$ , and  $(\frac{9\pi}{12}, \frac{11\pi}{12})$ . Each of the six size parameters was then plotted vs. the reaction plane orientation for a given centrality and  $k_T$  bin. The dependence was fit with the formula (5) including only the allowed oscillations, and the fit values were corrected for the finite bin size [65]. By symmetry arguments, the oscillations in the *long*, *side-long* and *out-long* components must vanish, as they do within statistical error in our calculations. This is the reason why they are not shown in the plot.

Fig. 3 shows a very good agreement for  $R_{\text{out},0}$  and  $R_{\text{side},0}$ , where the model points are close to the experiment at all centralities and  $k_T$  bins. The agreement for  $R_{\text{long},0}^2$  is somewhat worse in the lowest  $k_T$  bin, with the model overshooting the data by up to 10% for the values of the radius itself. This may be due to the assumed exact boost invariance in the model calculation. The oscillations  $R_{\text{side},2}^2$  and  $R_{\text{out},2}^2$  are in a very good agreement with the data. The oscillations in the cross term  $R_{\text{out-side}}$  are about 50% above the data. This mismatch requires explanation.

### B. Gaussian vs. Glauber initial condition

In order to point out the relevance of the initial condition mentioned in Ref. [24], we compare in Fig. 4 the angle-averaged *side*, *out*, and *long* radii, and the ratio  $R_{\text{out}}/R_{\text{side}}$ , obtained with the Glauber and Gaussian initial conditions. We note a much better agreement with the presently applied Gaussian initial condition. In particular, the ratio  $R_{\text{out}}/R_{\text{side}}$  coincides now with the experiment, while with the Glauber profile it was about 20% above the data and the  $k_T$ -dependence was not reproduced.

### C. Predictions for LHC

In Fig. 5 we show a plot analogous to Fig. 3 but with calculations done for the LHC energies, assuming the initial temperature of 500 MeV. As expected, the larger radii reflect the growth of the overall size of the system at freeze-out. All three radii grow, but the *out* radius seems to grow less, which is discussed in detail later. Also the azimuthal oscillations relative to  $R_{\text{side}}^2$  are smaller compared to RHIC. Again, this is expected: the initial asymmetry of the system at a given centrality is quite similar at RHIC and at the LHC, since it is mainly driven by the overlap geometry of the two colliding nuclei. The system then evolves from the out-of-plane extended source towards the more spherical shape, and if the evolution time is long enough, it may eventually overshoot and become in-plane extended. Measurements at RHIC show

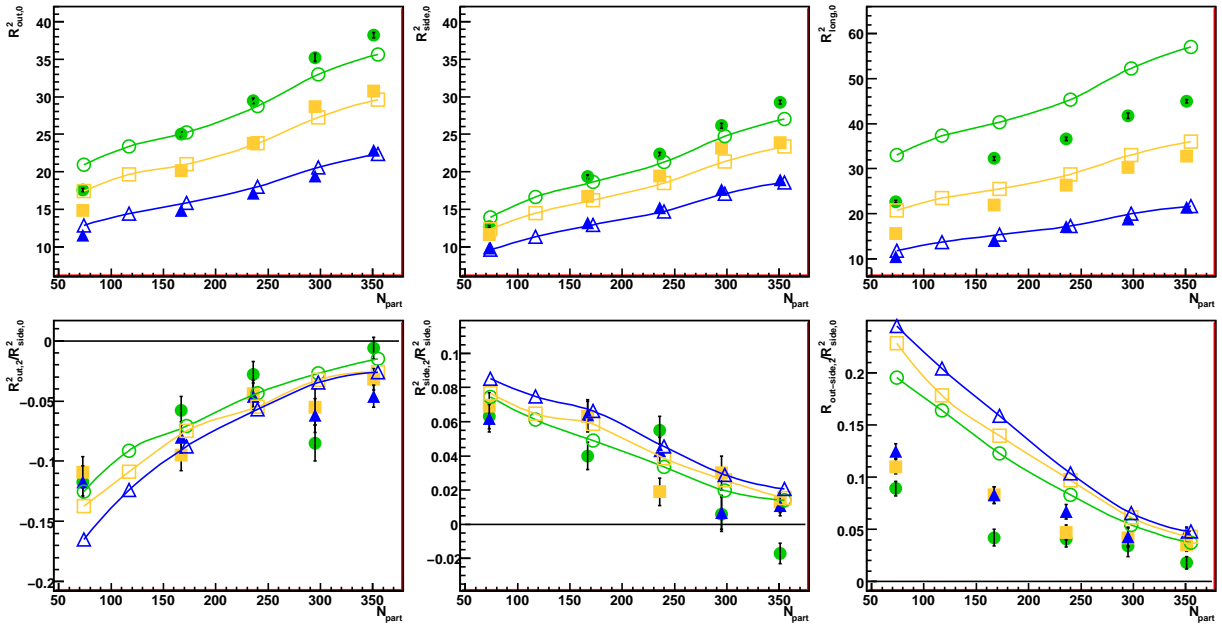


FIG. 3: (Color online) Results for the RHIC HBT radii and their azimuthal oscillations. For each value of  $N_{\text{part}}$  on the horizontal axis we plot the experimental points (filled symbols) and the model results (empty symbols). The points from top to bottom at each plot correspond to  $k_T$  contained in the bins 0.15-0.25 GeV (circles), 0.25-0.35 GeV (squares), and 0.35-0.6 GeV (triangles). The top panels show  $R_{\text{out},0}^2$ ,  $R_{\text{side},0}^2$ , and  $R_{\text{long},0}^2$ , the bottom panels the magnitude of the allowed oscillations divided conventionally by  $R_{\text{side},0}^2$ . Data from Ref. [66].

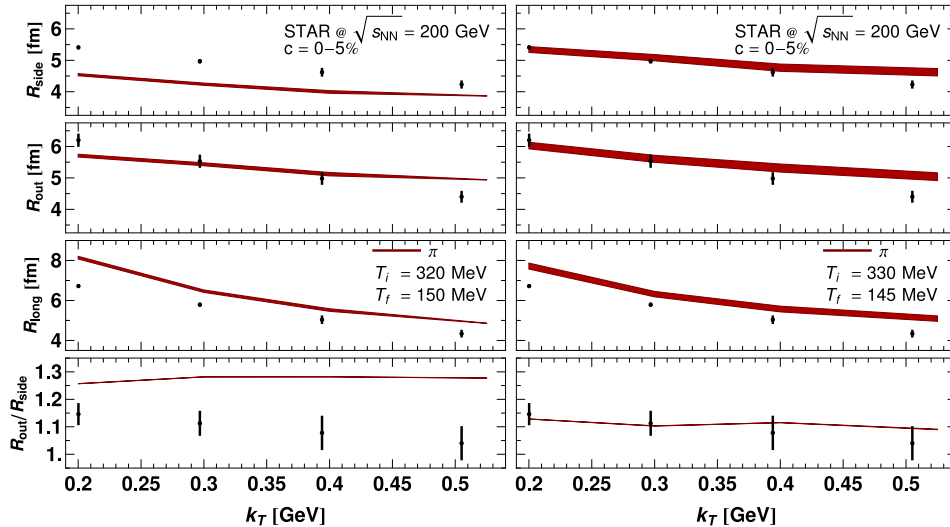


FIG. 4: (Color online) Results for the angle-averaged side, *out*, and *long* radii, and the ratio  $R_{\text{out}}/R_{\text{side}}$ , for the Glauber initial condition (left) and for the Gaussian initial condition (right). Data from Ref. [66].

that the source freezes out while still in the out-of-plane shape. Our calculations for LHC show that the evolution time to freeze-out is longer, but not long enough to produce the overshoot. The smaller oscillations (relative to  $R_{\text{side}}^2$ ) are a consequence of the fact that the system has been evolving for a longer time and effectively becomes more spherical than at RHIC.

In Fig. 6 we show an example comparison of the  $k_T$  dependence of the radii at RHIC and LHC energies at one of the centralities (in this case top 5%). Two main features

are apparent: the overall increase of the system size as well as larger gradient (steeper slope) of transverse radii considered as functions of  $k_T$ . The latter is a consequence of the larger averaged transverse flow developed at the LHC. This is illustrated in Fig. 2 - compare the numbers indicating transverse velocity at freeze-out on panels b) and c). The cause for the former was already discussed, now we concentrate on one particular feature. While the overall size of the system is indeed larger at the LHC, the radii do not seem to grow in the same way. The *out* radius

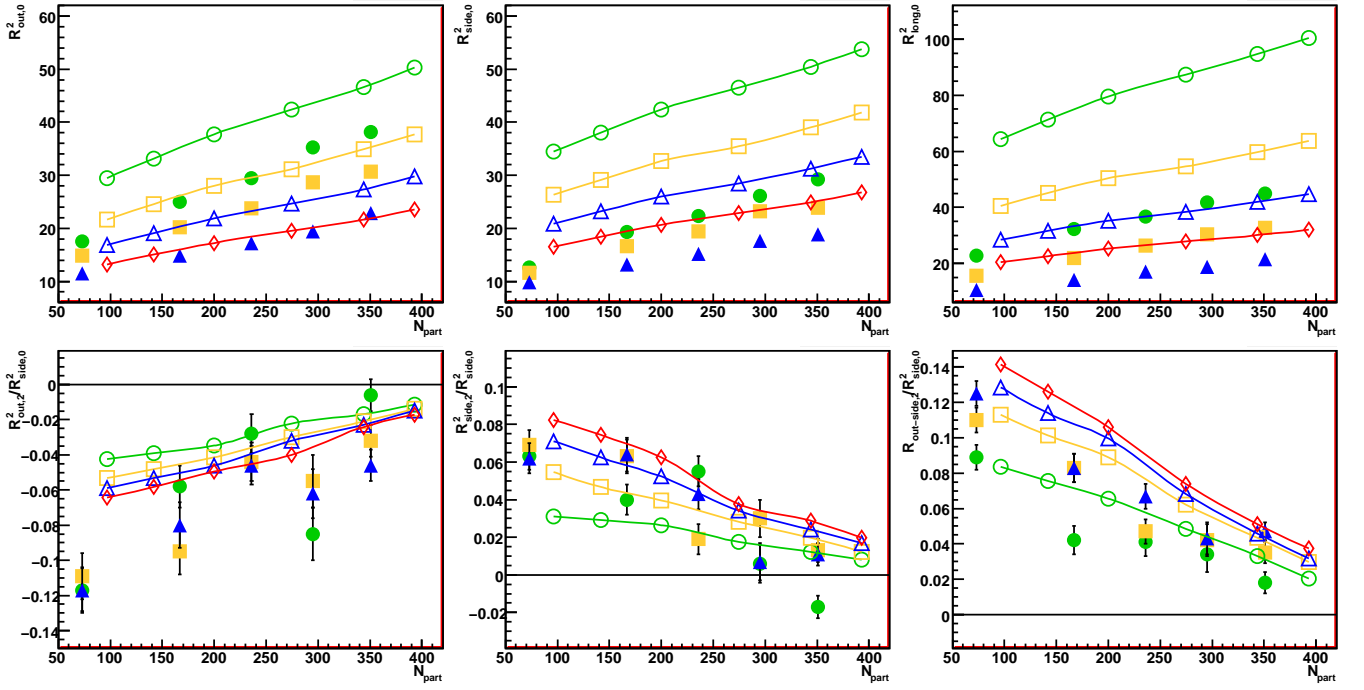


FIG. 5: (Color online) Predictions for the LHC. Filled symbols are RHIC data from STAR, shown for comparison (circles -  $k_T$  in 0.15-0.25 GeV, squares -  $k_T$  in 0.25-0.25 GeV, triangles -  $k_T$  in 0.35-0.6 GeV). Open symbols are the results of our calculation for the LHC energy with the initial temperature set to 500 MeV. The last  $k_T$  bin has been divided into two: open triangles -  $k_T$  in 0.35-0.45 GeV and open diamonds -  $k_T$  in 0.45-0.6 GeV. Top panels show sizes (squared) averaged over the  $\phi$  angle. Bottom panels show magnitude of the allowed oscillations, divided by  $R_{side}^2$ . Data from Ref. [66].

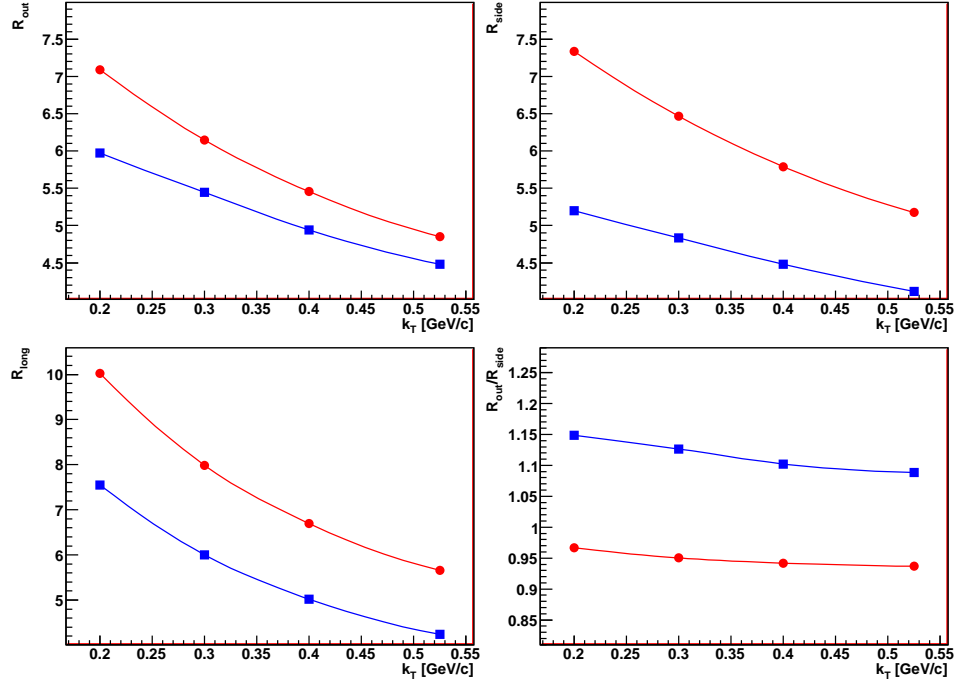


FIG. 6: (Color online) Comparison of calculations for the top 5% central AuAu collisions at RHIC (squares) and PbPb collisions at LHC (circles) energies. Lines are drawn to guide the eye. Top-left panel shows *out* radius, top-right - *side* radius, bottom left - *long* radius, bottom right - *out* over *side* radii ratio.

grows significantly less than the other two, which is best illustrated by the  $R_{out}/R_{side}$  ratio, which decreases from

1.1 at RHIC to 0.95 at the LHC. It comes from a qualitative change in the results of the hydrodynamic calculation

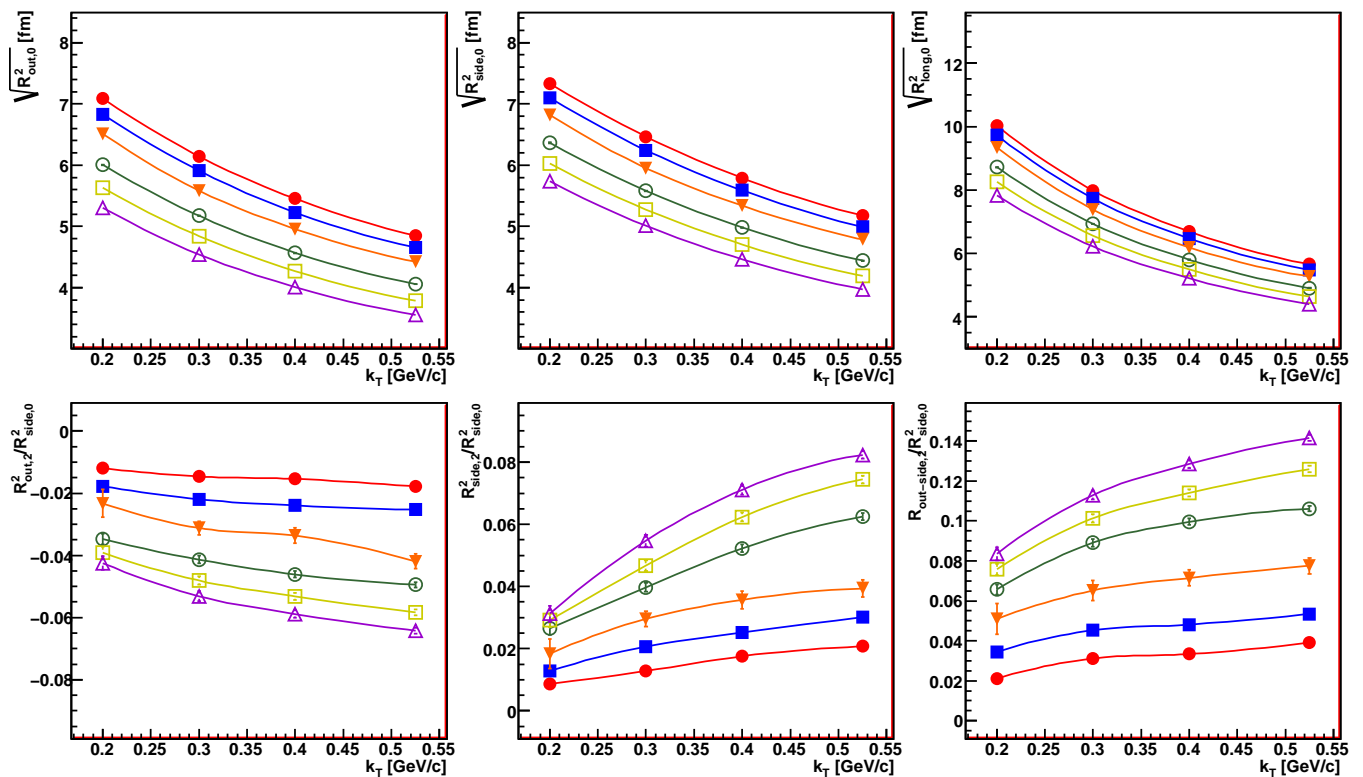


FIG. 7: (Color online) Calculations for the LHC with the Gaussian initial conditions for 6 centralities (filled circles - 0-5%, filled squares - 5-10%, filled down triangles 10-20%, open circles - 20-30%, open squares - 30-40%, open up triangles - 40-50%). Upper plots show the  $\phi$ -averaged radii (from left to right:  $R_{out}$ ,  $R_{side}$ ,  $R_{long}$ , lower plots show the magnitude of the allowed oscillations (from left to right  $R_{out,2}^2$ ,  $R_{side,2}^2$ ,  $R_{out-side,2}$ ), all as functions of the pair transverse-momentum  $k_T$ .

seen in Fig. 2. At RHIC the hypersurface at freeze-out temperatures was “outside-in”, or in other words particles at the larger transverse distances froze out earlier. We refer the reader to our previous work [30] where this effect was studied in the simplified form by analyzing the modified Blast-wave parametrization. The RHIC data were found to be consistent with the so-called “negative a” scenario, that is the “outside-in” freeze-out, which is also consistent with our more detailed hydrodynamic calculation, and other hydrodynamic calculations. On the other hand the so-called “positive a”, or “inside-out” scenario was inconsistent with the data mainly due to too small  $R_{out}$ . The detailed hydrodynamics calculation for LHC energies shown in this work exhibit a qualitative change in the freeze-out shape to the “inside-out” type. Therefore we do expect to see a smaller, or more precisely, less increased outwards radii, and that is exactly what we see in Fig. 6. The effect is large, when compared with the expected experimental systematic uncertainties and therefore can be easily tested. Its confirmation in the data would be a very strong indication of the existence of the hydrodynamically behaving medium in relativistic heavy-ion collisions, and would indicate that we are significantly advanced in understanding the dynamics of this medium.

#### D. LHC results as function of $k_T$

In Fig. 7 we show the azimuthally sensitive HBT results for the LHC energies as a function of the pair transverse momentum  $k_T$ , including the low momentum bin of 0.05 – 0.15 GeV. The *out* and *side* radii fall with  $k_T$  in a similar way, linearly. The expected decrease of the size with growing centrality is also apparent, while the  $R_{out}/R_{side}$  ratio is close to a constant for all centralities and values of  $k_T$ . The *long* radius also falls as expected. In general, the trends in the radii, plotted both versus centrality and  $k_T$ , are smooth and well understood. It is interesting to note the behavior of the oscillations. Their sign is the same as for LHC as for RHIC. Although we do see a decrease in the magnitude of oscillations with lowering  $k_T$ , especially in the *side* direction, they do not change sign. Also the magnitude of the oscillations grows consistently with increasing centrality for all  $k_T$  bins.

The oscillations obtained from the analysis of the HBT correlation functions correspond to the system asymmetry at the final stages of the collision, when the freeze-out occurs. It is interesting to compare them to the initial space asymmetry, as obtained from the Glauber calculations and presented in Tab. I. This is shown in Fig. 8. One can see that after dividing the observed asymmetry by its initial value one obtains a curve which appears to



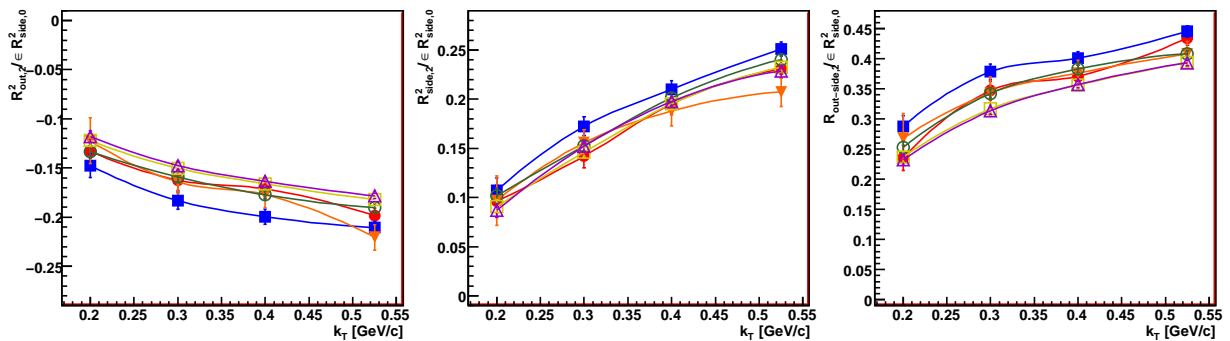


FIG. 8: (Color online) Scaled azHBT oscillations for the LHC initial conditions for 6 centralities (filled circles - 0-5%, filled squares - 5-10%, down triangles 10-20%, open circles - 20-30%, open squares - 30-40%, up triangles - 40-50%). The symbols show the magnitude of the allowed oscillations (from left to right:  $R_{out,2}^2$ ,  $R_{side,2}^2$ ,  $R_{out-side,2}^2$ ) divided by the initial eccentricity  $\epsilon$  from Table I and by  $R_{side}^2$ .

be universal, within the statistical uncertainties of this study, for all considered centralities.

### E. Emission history

The above considerations constitute an overall picture that can be deduced from the radii alone. However, since the particles are emitted during the whole evolution time, the observed shape is essentially a multiplicity-weighted average of the shape evolution of the system at subsequent times. An example of such shape evolution with indicated birth points of the primary pions is shown in Fig. 9 for the 20-30% centrality for the PbPb collisions at LHC. The information discussed below is a more detailed analysis of the behavior which may be inferred from Fig. 2. The panels in Fig. 9 show where the charged primordial pions are emitted in a given time interval. The scale (shown in the bottom-right panel) indicates how many pions are emitted from a given area element in the transverse plane. The picture shows the slice centered at midrapidity (the  $z$  coordinate of the particle emission satisfies the condition  $|z| < 1$  fm). At the very beginning of the collision ( $t < 1.0$  fm) there are no particles emitted. However, we observe particle emission at the very early stage - already in the first time slice (1.0-1.7 fm). Obviously the system has only begun its evolution, hence the shape is still very much out-of-plane extended, reflecting the initial overlap geometry. We also see that up to the very last evolution stage the emission is only from the surface of the system. As the evolution progresses particles are emitted from more and more spherical shells, up to the time of 9.7 fm. At this moment system reaches the freeze-out temperature in its full volume and emission changes its nature from the surface-like shell emission to the bulk emission from the whole volume. It is especially interesting to look at panel 10 (9.7-10.7 fm). One can see that the volume emission starts in the center of the system first, this is a very good illustration of the “inside-out” type of emission discussed earlier. What is also interesting is that even though the overall shape

of the system is very much in-plane extended, the inner emitting part has an out-of-plane shape. In the final stage of the evolution (panel 11: 10.7 - 11.7 fm) the volume emission continues and finally the outer parts of the system emit particles. As can be seen from the picture and the discussion, the emission patterns coupled to the shape evolution of the system are quite complex. There is no way to tell, a priori, what will be the overall system shape seen by femtoscopy. One must perform a detailed simulation of all the evolution stages, which must also include a realistic simulation of the number of particles coming from each stage of the evolution. This is precisely what we have done in this work.

In Fig. 10 we show the analog of Fig. 9, but with all pions, not only the primordial ones. We note that the resonance decays “wash out” the production regions, which is effectively increasing the size. This is due to the transverse flow, which has a tendency to carry out the resonance outward before it decays into pions. Qualitative conclusions concerning the surface and volume emission are the same as for Fig. 9. We also note that pion emission continues well past the time of 11.7 fm, as resonances with longer lifetimes subsequently decay. The detailed discussion of the influence of strongly decaying resonances on the HBT correlation functions and extracted radii can be found in [30].

## IV. CONCLUSIONS

The results presented in this paper show that it is possible to achieve a uniform description of the RHIC soft-hadronic data including azimuthally sensitive HBT radii. The initial space asymmetry of the source, tuned earlier to reproduce the value of  $v_2$ , turns out to be precisely such that the azimuthal dependence of  $R_{side,2}^2$  and  $R_{out,2}^2$  is also very well described. This verifies good consistency of our approach consisting of relativistic hydrodynamics and statistical hadronization – only the model prediction for the *out-side* radius is significantly different from the data, which requires explanation. For the LHC energy

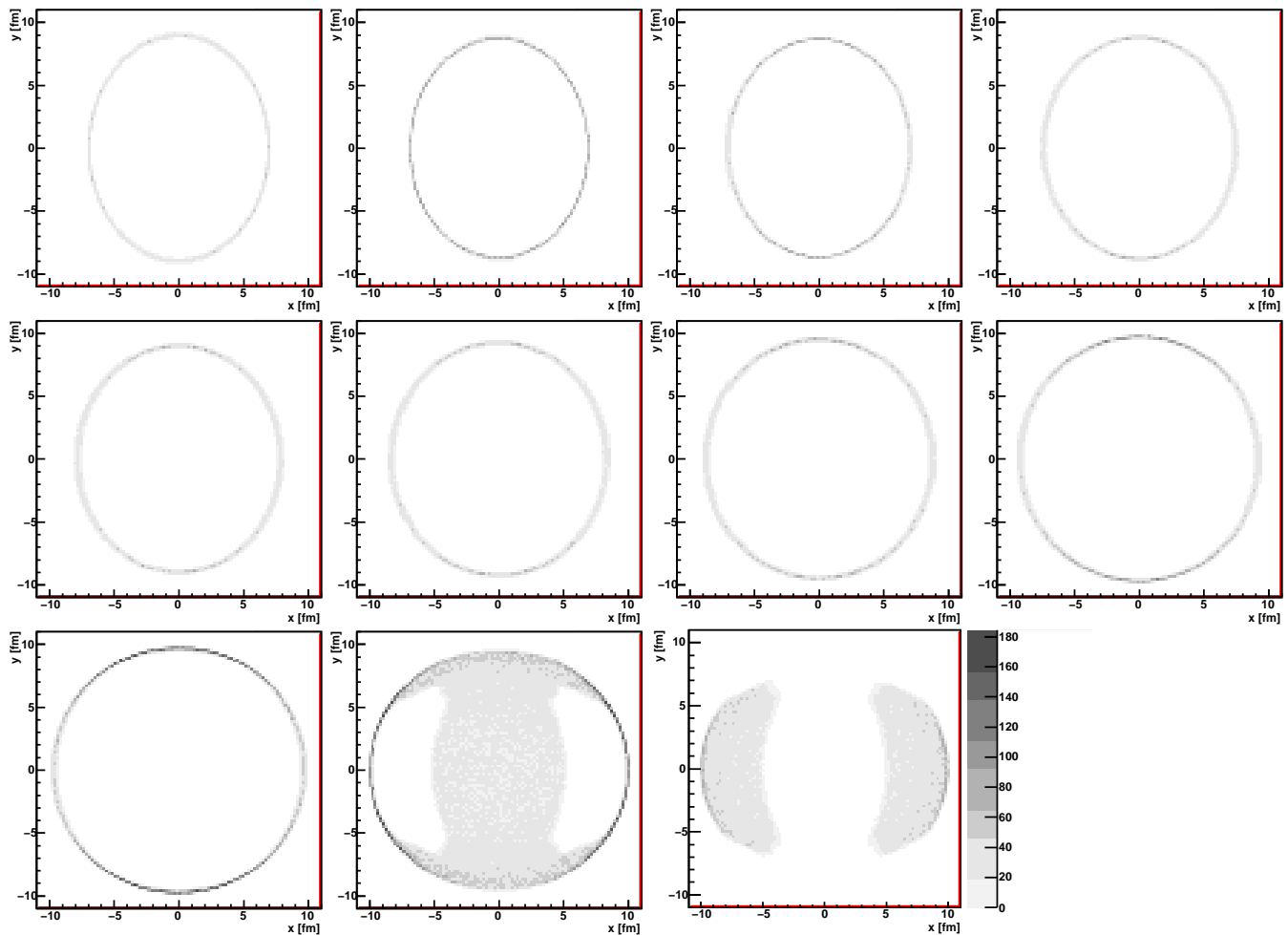


FIG. 9: Evolution of the shape of the system with time for the LHC energy and centrality 20-30%, as marked with the produced primordial pions. Each panel shows the birth places of primordial charged pions emitted in a time interval of duration 1 fm. The pions originate from the region placed at the center of the collision ( $|z| < 1$  fm). The top-left panel corresponds to the time interval 1.0-1.7 fm, top middle-left to 1.7-2.7 fm, and so on up to the time interval 10.7-11.7 fm shown in the lower-right panel. The shades of gray indicate the relative number of primordial charged pions emitted from the area element in the transverse  $(x, y)$  plane within the given time interval.

we predict the moderate increase of the HBT radii and the decrease of their azimuthal oscillations. Such effects can be naturally explained by longer evolution times at LHC. The space-time patterns of particle emission were discussed in detail. They indicate that the shape of the system seen by the femtoscopic methods is an average of the complex and varying in time shape of the emitting source.

In summary, the results of our calculations for RHIC and LHC conditions show several notable features. First of all the calculations for RHIC show a remarkable agreement with the broad spectrum of the soft physics data. We have concentrated on the transverse dynamics of the source, and our model appears to properly describe not only the momentum part of the observed phase space, but also the space-time part. The unique feature of the model is the proper description of the azimuthal asymmetry in the *side* and *out* directions, again both in the momen-

tum and space-time, which has been achieved before only in simplified and non-dynamical blast-wave parametrizations [23] which neglect the important contributions of the strongly decaying resonances, as well as the surface emission. The underlying hypothesis of our work is that the system created in heavy-ion collisions at RHIC behaves as a single piece of matter, and can be described by the hydrodynamic equations. These equations include the state-of-the-art equation of state which assumes that the matter above a certain critical temperature is in a deconfined phase (Quark Gluon Plasma). In our calculation the evolving system at RHIC spends a significant amount of time in that phase, and its properties are essential in shaping up the final observables. This work provides another crucial confirmation that such a hypothesis is consistent with the experimental data. While in itself it does not constitute a proof that the Quark Gluon Plasma is indeed created at RHIC, we stress that any alternative

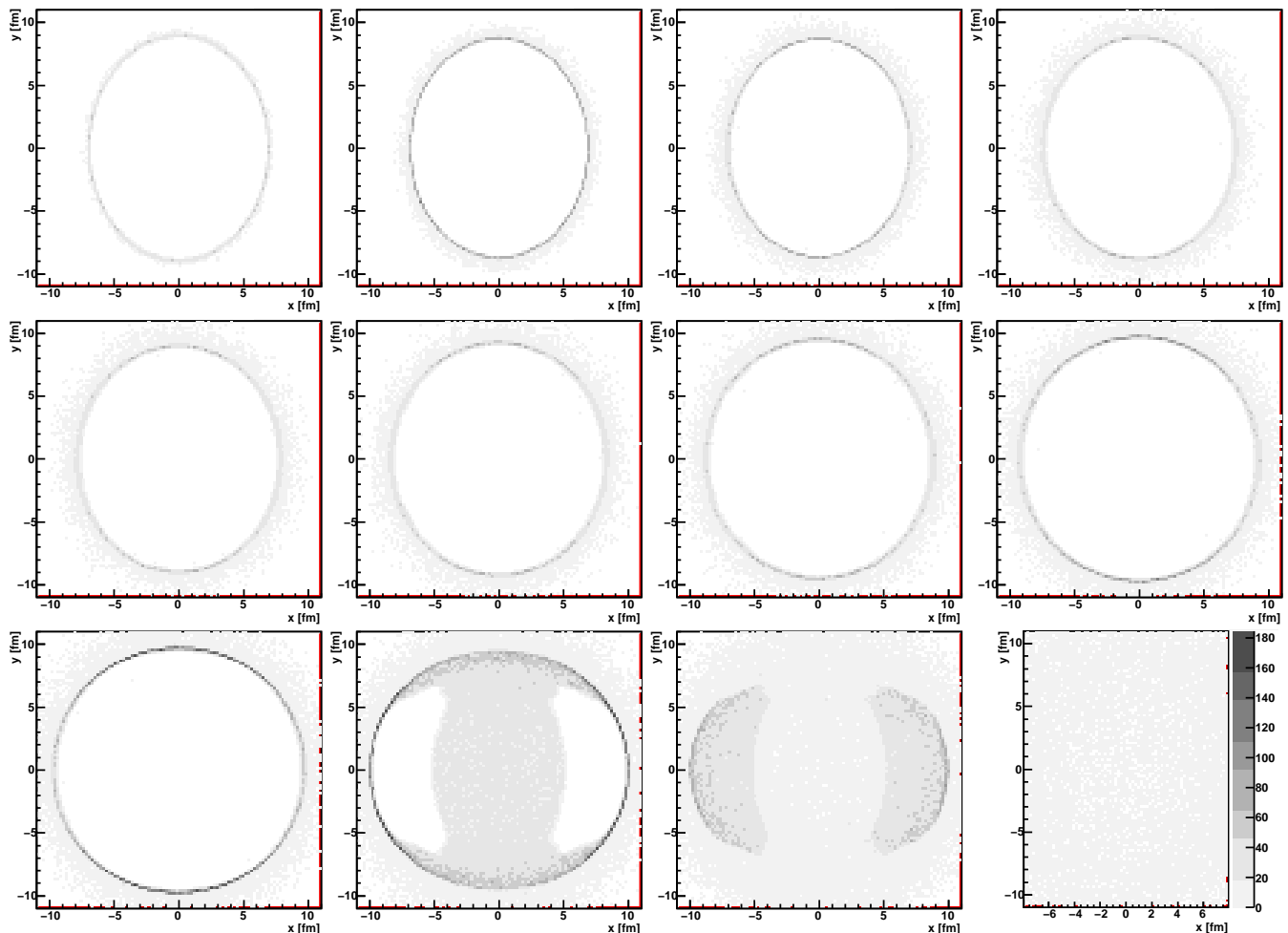


FIG. 10: Same as Fig. 9 for all pions, primordial and from resonance decays.

explanation must at least achieve a similar agreement with the experimental data to be considered viable.

The system created in heavy ion collisions at the LHC is predicted to be in many ways similar to the one created at RHIC, at least in the sense that it also is expected to spend a long time in the deconfined phase. In fact, this time is predicted to be significantly larger than at RHIC, such that its influence on the final observables may be more pronounced. Again, we work under the assumption that hydrodynamics provides a good description of the matter in such conditions, which allows us to provide predictions for final state observables at these energies. We stress that the underlying mechanisms of the model do not change at all between the RHIC and the LHC energies, only a few of the external parameters, such as the initial nucleon-nucleon cross-section or the initial temperature are changed in a reasonable way.

Nevertheless, we are able to identify significant changes in the observables (with respect to RHIC) that can be easily measured in the LHC experiments. In particular in this work, which focuses on femtoscopy, we have identified two of them which are particularly sensitive: the decrease of final observed anisotropy of the source (relative to  $R_{side}^2$ ), reflected in the decrease of the oscillations in  $R_{out}$  and  $R_{side}$  radii, and the change from the “inside-out” to the “outside-in” type of freeze-out, reflected in the femtoscopic radii themselves and best illustrated as the decrease of the  $R_{out}/R_{side}$  ratio. These features are specific enough such that they provide strict tests of the validity of the hydrodynamic hypothesis. If observed, they will be a strong argument that systems at RHIC and the LHC can indeed, at least in the soft sector, be described by essentially the same physics principles.

[1] M. A. Lisa, S. Pratt, R. Soltz, and U. Wiedemann, *Ann. Rev. Nucl. Part. Sci.* **55**, 357 (2005), nucl-ex/0505014.

[2] R. Hanbury Brown and R. Q. Twiss, *Phil. Mag.* **45**, 663 (1954).

- [3] R. Hanbury Brown and R. Q. Twiss, *Nature* **178**, 1046 (1956).
- [4] G. Goldhaber, S. Goldhaber, W.-Y. Lee, and A. Pais, *Phys. Rev.* **120**, 300 (1960).
- [5] M. Gyulassy, S. K. Kauffmann, and L. W. Wilson, *Phys. Rev.* **C20**, 2267 (1979).
- [6] S. V. Voloshin, LBNL annual report R20 (1998), <http://ie.lbl.gov/nsd1999/rnc/RNC.htm>.
- [7] M. A. Lisa et al. (E895), *Phys. Lett.* **B496**, 1 (2000), nucl-ex/0007022.
- [8] J.-Y. Ollitrault, *Phys. Rev.* **D46**, 229 (1992).
- [9] U. W. Heinz and P. F. Kolb (2002), hep-ph/0204061.
- [10] T. Hirano, *Acta Phys. Polon.* **B36**, 187 (2005), nucl-th/0410017.
- [11] P. Huovinen and P. V. Ruuskanen, *Ann. Rev. Nucl. Part. Sci.* **56**, 163 (2006), nucl-th/0605008.
- [12] U. W. Heinz and P. F. Kolb, *Nucl. Phys.* **A702**, 269 (2002), hep-ph/0111075.
- [13] T. Hirano, K. Morita, S. Muroya, and C. Nonaka, *Phys. Rev.* **C65**, 061902 (2002), nucl-th/0110009.
- [14] T. Hirano and K. Tsuda, *Nucl. Phys.* **A715**, 821 (2003), nucl-th/0208068.
- [15] D. Zschesche, S. Schramm, H. Stoecker, and W. Greiner, *Phys. Rev.* **C65**, 064902 (2002), nucl-th/0107037.
- [16] J. Socolowski, O., F. Grassi, Y. Hama, and T. Kodama, *Phys. Rev. Lett.* **93**, 182301 (2004), hep-ph/0405181.
- [17] U. W. Heinz and P. F. Kolb, *Phys. Lett.* **B542**, 216 (2002), hep-ph/0206278.
- [18] B. Tomasik, *Acta Phys. Polon.* **B36**, 2087 (2005), nucl-th/0409074.
- [19] B. Tomasik, *AIP Conf. Proc.* **828**, 464 (2006), nucl-th/0509100.
- [20] T. J. Humanic, *Int. J. Mod. Phys.* **E15**, 197 (2006), nucl-th/0510049.
- [21] E. Frodermann, R. Chatterjee, and U. Heinz, *J. Phys.* **G34**, 2249 (2007), 0707.1898.
- [22] M. Csanad, B. Tomasik, and T. Csorgo (2008), 0801.4434.
- [23] F. Retiere and M. A. Lisa, *Phys. Rev.* **C70**, 044907 (2004), nucl-th/0312024.
- [24] W. Broniowski, M. Chojnacki, W. Florkowski, and A. Kisiel (2008), 0801.4361.
- [25] A. Kisiel, T. Taluc, W. Broniowski, and W. Florkowski, *Comput. Phys. Commun.* **174**, 669 (2006), nucl-th/0504047.
- [26] G. Torrieri et al., *Comput. Phys. Commun.* **167**, 229 (2005), nucl-th/0404083.
- [27] M. Chojnacki, W. Florkowski, W. Broniowski, and A. Kisiel (2007), 0712.0947.
- [28] M. Chojnacki and W. Florkowski, *Phys. Rev.* **C74**, 034905 (2006), nucl-th/0603065.
- [29] M. Chojnacki and W. Florkowski, *Acta Phys. Polon.* **B38**, 3249 (2007), nucl-th/0702030.
- [30] A. Kisiel, W. Florkowski, and W. Broniowski, *Phys. Rev.* **C73**, 064902 (2006), nucl-th/0602039.
- [31] W. Broniowski, M. Rybczynski, and P. Bozek (2007), arXiv:0710.5731 [nucl-th].
- [32] R. Andrade, F. Grassi, Y. Hama, T. Kodama, and J. Socolowski, O., *Phys. Rev. Lett.* **97**, 202302 (2006), nucl-th/0608067.
- [33] Y. Hama et al. (2007), 0711.4544.
- [34] L. D. McLerran and R. Venugopalan, *Phys. Rev.* **D49**, 2233 (1994), hep-ph/9309289.
- [35] L. D. McLerran and R. Venugopalan, *Phys. Rev.* **D49**, 3352 (1994), hep-ph/9311205.
- [36] D. Kharzeev, E. Levin, and M. Nardi, *Phys. Rev.* **C71**, 054903 (2005), hep-ph/0111315.
- [37] S. Mrowczynski, *Phys. Lett.* **B314**, 118 (1993).
- [38] B. Muller, *Acta Phys. Polon.* **B38**, 3705 (2007), 0710.3366.
- [39] D. Kharzeev and M. Nardi, *Phys. Lett.* **B507**, 121 (2001), nucl-th/0012025.
- [40] A. Bialas, M. Bleszynski, and W. Czyz, *Nucl. Phys.* **B111**, 461 (1976).
- [41] B. B. Back et al. (PHOBOS), *Phys. Rev.* **C65**, 031901 (2002), nucl-ex/0105011.
- [42] B. B. Back et al. (PHOBOS), *Phys. Rev.* **C70**, 021902 (2004), nucl-ex/0405027.
- [43] W. M. Yao et al. (Particle Data Group), *J. Phys.* **G33**, 1 (2006).
- [44] W. Broniowski, P. Bozek, and M. Rybczynski, *Phys. Rev.* **C76**, 054905 (2007), 0706.4266.
- [45] P. Braun-Munzinger, D. Magestro, K. Redlich, and J. Stachel, *Phys. Lett.* **B518**, 41 (2001), hep-ph/0105229.
- [46] W. Broniowski and W. Florkowski, *Phys. Rev. Lett.* **87**, 272302 (2001), nucl-th/0106050.
- [47] W. Broniowski and W. Florkowski, *Phys. Rev.* **C65**, 064905 (2002), nucl-th/0112043.
- [48] J. Rafelski, J. Letessier, and G. Torrieri, *Phys. Rev.* **C72**, 024905 (2005), nucl-th/0412072.
- [49] D. Prorok (2007), nucl-th/0702042.
- [50] E. Schnedermann, J. Sollfrank, and U. W. Heinz, *Phys. Rev.* **C48**, 2462 (1993), nucl-th/9307020.
- [51] K. A. Bugaev, *Nucl. Phys.* **A606**, 559 (1996), nucl-th/9906047.
- [52] C. Anderlik et al., *Phys. Rev.* **C59**, 3309 (1999), nucl-th/9806004.
- [53] M. S. Borysova, Y. M. Sinyukov, S. V. Akkelin, B. Erasmus, and I. A. Karpenko, *Phys. Rev.* **C73**, 024903 (2006), nucl-th/0507057.
- [54] Y. M. Sinyukov, *Acta Phys. Polon.* **B37**, 3343 (2006).
- [55] M. Gyulassy, Y. M. Sinyukov, I. Karpenko, and A. V. Nazarenko, *Braz. J. Phys.* **37**, 1031 (2007).
- [56] F. Cooper and G. Frye, *Phys. Rev.* **D10**, 186 (1974).
- [57] D. Teaney, J. Lauret, and E. V. Shuryak, *Phys. Rev. Lett.* **86**, 4783 (2001), nucl-th/0011058.
- [58] C. Nonaka and S. A. Bass, *Phys. Rev.* **C75**, 014902 (2007), nucl-th/0607018.
- [59] T. Hirano, U. W. Heinz, D. Kharzeev, R. Lacey, and Y. Nara, *J. Phys.* **G34**, S879 (2007), nucl-th/0701075.
- [60] N. S. Amelin et al., *Phys. Rev.* **C74**, 064901 (2006), nucl-th/0608057.
- [61] M. G. Bowler, *Phys. Lett.* **B270**, 69 (1991).
- [62] Y. Sinyukov, R. Lednicky, S. V. Akkelin, J. Pluta, and B. Erasmus, *Phys. Lett.* **B432**, 248 (1998).
- [63] S. Pratt, *Phys. Rev.* **D33**, 1314 (1986).
- [64] G. F. Bertsch, *Nucl. Phys.* **A498**, 173c (1989).
- [65] U. W. Heinz, A. Hummel, M. A. Lisa, and U. A. Wiedemann, *Phys. Rev.* **C66**, 044903 (2002), nucl-th/0207003.
- [66] J. Adams et al. (STAR), *Phys. Rev. Lett.* **93**, 012301 (2004), nucl-ex/0312009.